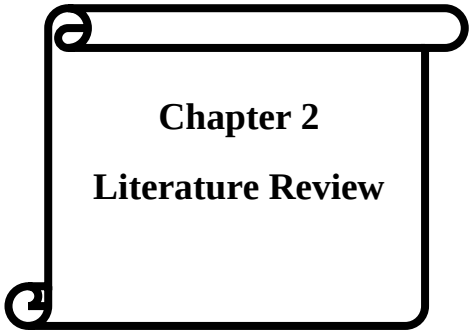
Chapter 2
Literature Review

There are different types of materials that can be used efficiently as supercapacitor electrode materials. Various conducting polymers such as polyaniline (PANI), polyacetylene (PA), polythiophene (PTh), polypyrrole (PPy), single and binary metal oxides such as CuO, NiO, MnO_2, Co_3O_4, Fe_3O_4, $CuFe_2O_4$ $FeCo_2O_4$, $NiCo_2O_4$, $MnCo_2O_4$, $ZnCo_2O_4$, $CoFe_2O_4$, $CuCo_2O_4$, carbon-based materials like activated carbon, CNTs, graphene have been extensively studied for the supercapacitor applications.

2.1 Conducting polymers

Conducting polymers are a class of organic polymers with the ability to conduct electricity. Traditional polymers, like polyethylene, bind the valence electrons via low mobility sp_3 hybridized covalent bonds (σ bonding). While conducting polymers exhibit magnificent electrochemical properties attributed to their delocalized π electrons. The overlap of carbon p_z orbitals, results in a continuous backbone of sp_2 hybridized carbon centres. This arrangement creates a conjugated -system characterized by alternating single and double bonds within the polymers. On each of the sp^2 centres, an unpaired valence electron is located in a p_z orbital that is orthogonal to the other three bonds and creates a bonding π band and corresponding antibonding π* band. An appropriate oxidant can take an electron from this band to create a positively charged "hole" (electron deficiency). As a result, the remaining electrons in the band will become more mobile and conductive. To achieve electroneutrality, polymer doping (also known as p-doping), an ion insertion procedure, must occur, which raises the redox state and electronic conductivity [47]. The reduction of these conjugated polymers theoretically adds an electron to a band that would not otherwise be filled (n-doping). In practical applications, most conductive polymers are primarily doped oxidatively to produce p-type materials, although n-doped polymers are also synthesized frequently [48].

Conducting polymers are enticing because of their high energy storage capacity, low cost, economy of production, lightweightness, and flexibility, allowing for a wide range of design possibilities. Conducting polymers store charge throughout the entire (accessible) volume via a fast doping/dedoping exchange of ions, whereas double-layer capacitors only store energy on the material's surface. Consequently, the amount of energy that can be stored with conducting polymers is typically higher compared to EDLC-type materials. Polymer-based materials are also more prone to lower self-discharge rates because they store charge through doping/dedoping (faradic) rather than adsorption/desorption (non-faradic).

One of the first conducting polymers is polyaniline (PANI), also known as aniline black historically, can be produced chemically or electrochemically. Interestingly, all of the initial works after the first report in 1886 were based on electropolymerization [49–51]. The high electrical conductivity of PANI and its potential electrochemical applications were introduced in 1968, about a decade before the seminal work of Heeger and his coworkers. This pivotal discovery paved the way for the emergence of conducting polymers and eventually led to the prestigious 2000 Nobel prize in chemistry. Diaz and coworkers described PANI's electrochemical behavior for the first time [52]. Since then, due to its electrochemical characteristics, polyaniline has attracted much attention from the research community from among all the conjugated polymers available due to the following reasons [53]. Among the various conjugated polymers available, PANI stands out for the following reasons:

(i) low cost

(ii) ease of synthesis and doping

(iii) tunable electrical conductivity and electronic structure

(iv) flexibility

(v) chemical and environmental stability

(vi) excellent yield from the polymerization of monomers

(vii) the presence of nitrogen atom occupies benzenoid and quinoid rings in the polymeric backbone, which is crucial for the formation of π bond and interchain electrical conduction

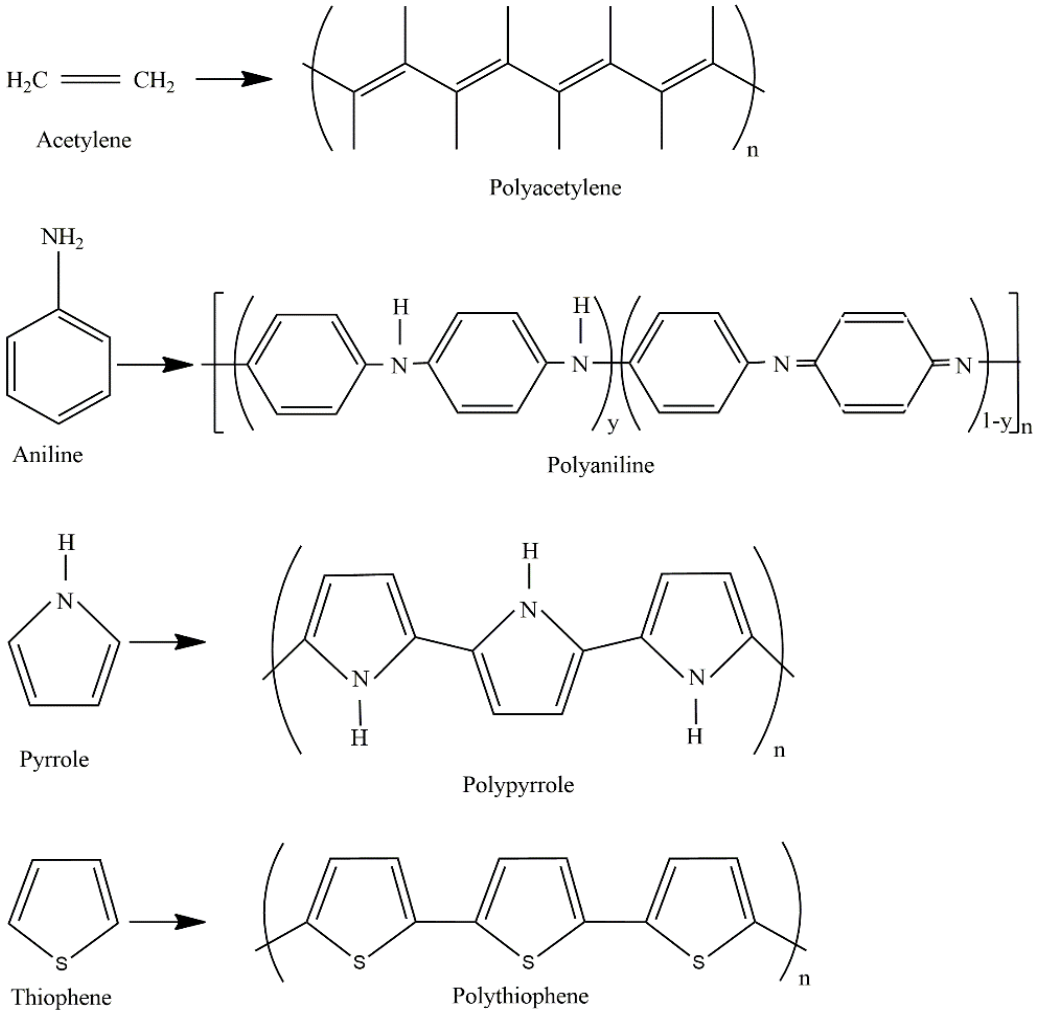

Fig 2.1: Different conducting polymers used for supercapacitor applications

The chemical structures of various conducting polymers have been shown in figure 2.1 [54].

2.2 Polyaniline (PANI)

Polyaniline exists in several distinct forms. The conducting properties of polyaniline is achieved through the process of doping, wherein specific dopants are used to induce various

oxidized and reduced states. These forms are named leucoemeraldine base (LB), emeraldine base (EB), emeraldine salt (ES), and pernigraniline base (PB), as shown in figure 2.2.

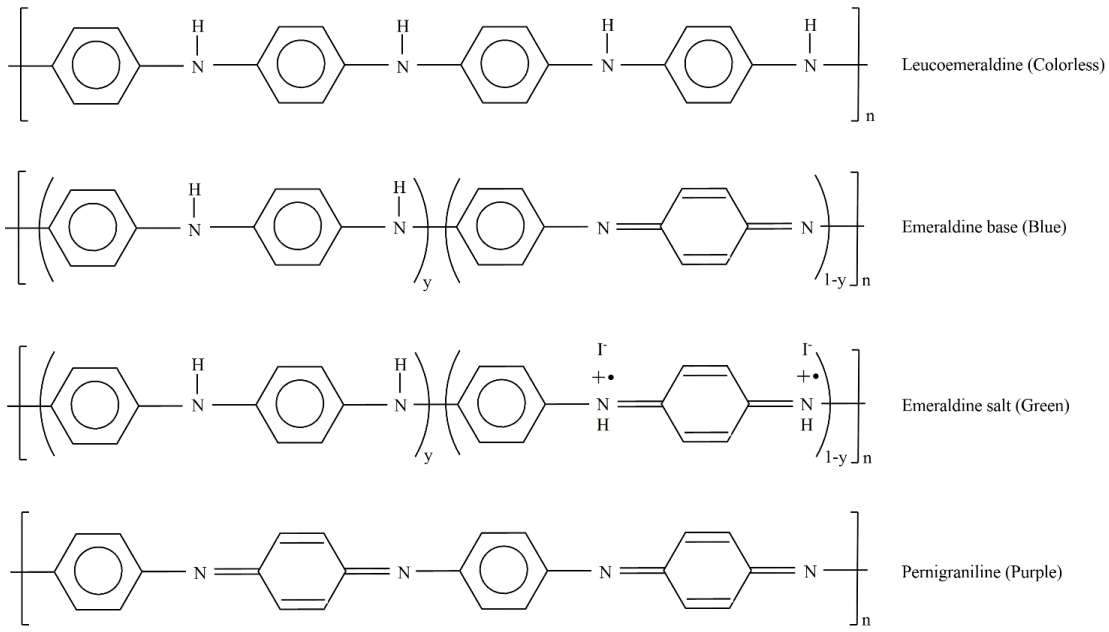

Fig 2.2: Different redox states of polyaniline

n = degree of polymerization

1-y = oxidation states (from 0 to 1)

1-y = 0 (colorless- fully reduced leucoemeraldine)

1-y = 0.5 (blue- semi-oxidized emeraldine base)

1-y = 1 (purple- fully oxidized pernigraniline)

Emeraldine salt is the most electrically conductive of all the states produced by protonating emeraldine base [55]. Chemical oxidative polymerization (COP), in which polymerization and doping occur concurrently, is the most popular, practical, straightforward, and affordable method of synthesizing polyaniline. In this process, an oxidizing agent is taken as initiator, taking a proton from aniline molecules to create defects and acids dopant [56,57]. The most

popular oxidants are $FeCl_3$, $AgNO_3$, $K_2Cr_2O_7$, APS (ammonium persulfate), and dopants include HCl, H_2SO_4, DBSA (dodecyl benzene sulfonic acid), CSA (camphorsulfonic acid), etc.

PANI has been investigated intensively owing to its high theoretical specific capacitance of 2000 F/g, ease of synthesis; high conductivity, multiple redox states, low cost, better environmental stability, fast doping, and de-doping kinetics. As a result of numerous advantages, it has proven its appropriateness in sensors, energy storage applications, plastic batteries, light-emitting diodes, etc. However, its compact morphology, poor processability and volumetric swelling tendency have restricted its applications to a large extent. Some of the results for PANI and PANI based composite materials have been discussed below:

Hu el al. [58] studied the effect of polymerization temperature on the electrochemical properties of polyaniline. They found that the PANI film polymerized at 4 °C exhibited the highest specific capacitance due to its lowest density of structural defects. M. Ates et al. in the year 2015, three synthesized binary composites PANI/ CuO, PEDOT/CuO, and Ppy/CuO and reported the specific capacitance values (at 5 mVs^{-1}) of 276.56 Fg^{-1}, 198.89 Fg^{-1}, and 20.78 Fg^{-1}, respectively. The capacitance values were reduced to 81.82 %, 68.55 %, and 48.39 % of initial values after 500 cycles, respectively [59]. Waikar et al. prepared polyaniline nanofibers with a surface area of 37.96 m^2 g^{-1} by electrodeposition of aniline-H_2SO_4 solution on flexible stainless substrate. The electrode fabricated from these nanofibers exhibited 473 Fg^{-1} specific capacitance at 5 mVs^{-1} with energy density and power density of 22 Wh kg^{-1} and 667 W kg^{-1} [60]. Mandal et al. prepared PANI/ $CoMoO_4$. 0.75 H_2O-based binary composite with the help of oxidative polymerization of aniline in the presence of $CoMoO_4$. 0.75 H_2O. The synthesized nanomaterial demonstrated 380 Fg^{-1} at a current density of 1 A g^{-1}. The cyclic stability test revealed that after 1000 continuous charge-discharge cycles at a constant current density of 1 Ag^{-1}, the specific capacitance retention was around 90.4%. The specific energy and power densities 42.7 Wh kg^{-1} and 450 W kg^{-1} were obtained[61]. Wang et al. thoroughly investigated

the effect of aniline concentration on crystallinity, morphology, chemical structure, and electrochemical properties. Dodecylbenzenesulfonic acid-doped polyaniline with an aniline concentration of 0.5 mol/L demonstrated the best electrochemical characteristics with a specific capacitance of 146 Fg^{-1} [62]. Li et al. prepared a three-dimensional (3D) strongly-coupled polyaniline/crosslinked carbon nanosheets (PANI/CCNs) composite with in-situ chemical polymerization technique using dopant HCl and oxidant APS. The assembled symmetric supercapacitor showed 72 F g^{-1} at 0.1 A g^{-1} current density. Further, the device exhibited energy and power density of 28.9 Wh kg^{-1} and 85.1 W kg^{-1} [63]. Yang et al. obtained a specific capacitance of 587.3 F g^{-1} at 0.1 A g^{-1} from optimal ternary composite based on polyaniline- manganese dioxide-carbon nanofiber. The ternary composite also demonstrated ~84 % charge retention after 1000 cycles at 10 A g^{-1}. Their research group used H_3PO_4 as a dopant and APS as an oxidant for the oxidative polymerization reaction [64]. Bian et al. prepared microporous polyaniline nanofibers with APS oxidant, reported a specific capacitance of 593 F g^{-1} at 2.5 A g^{-1} in 1 M H_2SO_4, and tested for 5000 cycles [65]. Khadry et al. fabricated electrodes from mesoporous-polyaniline films which incurred a specific capacitance of 532 F g^{-1} compared to 228 F g^{-1} for non-mesoporous polyaniline films which is a significant increase in electrochemical performance [66]. Liu et al. synthesized hierarchical composites of polyaniline- graphene nanoribbons- carbon nanotubes as electrode material which showed a specific capacitance of 890 Fg^{-1} compared to neat polyaniline of 283 Fg^{-1}. The composite also displayed cycling stability with a retention of 89 % after 1000 cycles [67]. Zhang et al. prepared polyaniline with HCl as a dopant and APS as an oxidant and then intercalated it into MnO_2 to form PANI-MnO_2. The maximum specific capacitance obtained from PANI-MnO_2 was 330 Fg^{-1} at 1 Ag^{-1}, an improvement of 76 % and 59 % as compared to pure PANI (187 Fg^{-1}) and MnO_2 (208 Fg^{-1}) [68]. Prasad et al. synthesized a solid-state redox supercapacitor with gel polymer as electrolyte and polyaniline as active material. A specific capacitance of 250 Fg^{-1}

was incurred at a specific power of 7.5 kW kg^{-1} [69]. Rahman et al. investigated the polyaniline nanofibers prepared from the green synthesis route and reported a specific capacitance of 832.5 Fg^{-1} and 528 Fg^{-1} at 1 Ag^{-1} and 40 Ag^{-1} current density. Also, their research group obtained a capacitance retention of 67.6 % of its initial value[70]. In another study, Li et al. utilized APS as oxidant and $HCLO_4$ as a dopant to form polyaniline nanofibers grown on the graphene surface. The specific capacitance obtained was 578 Fg^{-1} at a current density of 1 Ag^{-1}. The asymmetric supercapacitor assembled with graphene nanosheets demonstrated an energy and power density of 18.8 Wh kg^{-1} and 1000 W kg^{-1} and a capacitance retention of 93 % after 10000 cycles [71]. Zhao et al., in their research, found while synthesizing polyaniline/ graphite nanoplate composite that using oxidant APS instead of $FeCl_3$ largely increased the actual polyaniline content, conductivity and conductivity and specific capacitance. The composite prepared with an aniline to APS molar ratio of 1 exhibited a balanced combination of high specific capacitance (180.5 Fg^{-1} at 20 mVs^{-1}) and good rate capability with capacitance retention of 78 % [72].

An organized compilation of the research work performed in pristine polyaniline (PANI) and its composite materials has been provided in Table 2.1.

Table 2.1: Electrochemical properties of polyaniline-based supercapacitors.

Sample	Morphology	Method	T (°C)	Dopant	Oxidant	C_{sp} (Fg^{-1})	Scan rate or Current density	E_{sp} (wh kg^{-1})	P_{sp} (w kg^{-1})	Cycle life	Ref.
PANI	Nano nest	EP	-	H_2SO_4	-	757 (3E)	5 mVs^{-1}	0.786	2810	-	[73]

PANI	PANI	PANI	PANI	PANI	PANI	PANI	PANI
Porous structure	Interconnected rods	Layered flowers	Nanobelt	Nanotubes	-	Nanofiber	Nanowires
COP	COP	COP	COP	COP	EP	COP	EP
0	0-4	0-4	0	0-5	-	0-4	-
H2SO4	HCl	HCl	HCl	Benzene tetracarboxylic acid	HCl and HClO4	HCl	$HClO_4$
APS	APS	APS	APS	APS	-	APS	-
419 (3E)	779 (3E)	272 (3E)	304.4 (3E)	107 (SSC)	-	302 (SC)	373.6 (3E)
1 Ag^{-1}	0.2 Ag^{-1}	1 Ag^{-1}	0.5 Ag^{-1}	0.2 Ag^{-1}	-	1 Ag^{-1}	0.1 Ag^{-1}
8.42	11.6	0.09	-	9.5	12.57	26.8	6.08
147.2	80.3	-	-	80	283	402.6	403
-	96% @5000 cycles	50% @1500 cycles	40.65% @1000 cycles	90.9 % @5000 cycles	73% @3000 cycles	84% @1000 cycles	73.9% @1000 cycles
[81]	[80]	[79]	[78]	[77]	[76]	[75]	[74]

PANI LEB/MW	PANI-SA hydrogel	PANI ES/MWN	PANI/CX	PANI/ aerogel	PANI PB/MWC	PANI	PANI/SW CNT	PANI/CN F	PANI	PANI
Nanotube s	Nanofiber	Nanotube s	Aggregate d particles	3D network	-	Interconn ected nano-bridge	Nanofiber s	Nanofiber s	Nanorods	Interlocke d particles
COP	COP	COP	COP	COP	COP	COP	IP	COP	COP	COP
0-5	4	0-4	0-5	4	0-4	5	-	0	0-4	0-4
HCl	-	HCl	HCl	-	HCl	Phytic acid	CSA	HCl	H_2SO_4	HCl
APS	APS	APS	APS	APS	APS	APS	-	APS	APS	APS
217 (3E)	252 (3E)	328 (3E)	612 (3E)	184 (3E)	139 (3E)	523 (3E)	355 (3E)	234 (3E)	455.1 (3E)	249 (SC)
5 mVs^{-1}	0.5 Ag^{-1}	5 mVs^{-1}	0.1 Ag^{-1}	0.5 Ag^{-1}	5 mVs^{-1}	0.25 Ag^{-1}	0.5 Ag^{-1}	1 Ag^{-1}	1 mVs^{-1}	-
-	-	-	13.6	3	-	7.75	7.9	32	-	31
-	-	-	70.1	41.6	-	45.56	200	500	-	18
-	71% @1000 cycles	-	87.6 % @1500 cycles	74% @1000 cycles	-	88% @10000 cycles	87.2% @5000 cycles	90% @1000 cycles	-	-
[87]	[90]	[87]	[89]	[88]	[87]	[86]	[85]	[84]	[83]	[82]

PANI/ MnO_2	PANI/ ACF	PANI	PANI/ BCN	PANI-5% CdO	PANI@TiO_2/Ti_3C_2T
3D porous	nanorods	film	nanosheets	Nanoflakes /nanoparticles	Nanoflakes
COP	ECD	GD	EDP	COP	COP
4	-	-	-	-	0-2
Phytic acid	H_2SO_4	-	-	HCl	HCl
APS	-	-	-	APS	APS
314 (3E)	296.3 (3E)	15.08 (3E)	672 (3E)	866	188.3 (3E)
1 Ag^{-1}	1 Ag^{-1}	0.05 mA cm^{-2}	1 Ag^{-1}	5 mVs^{-1}	10 mVs^{-1}
23.2	30.42	-	25.3	9.04	-
720	900	-	10000	1510	-
86.5 % @ 2000 cycles	89.7 % @ 2000 cycles	97 % @ 500 cycles	89.6 % 10000 cycles	90.6 % @ 20000 cycles	94% @8000 cycles
[96]	[95]	[94]	[93]	[92]	[91]

Polyaniline (PANI) due to its low cost, ease of synthesis, multiple redox states and highly conducting nature has been mostly synthesized with the help of chemical oxidative polymerization which is more straightforward and affordable as compared to other techniques. However, owing to its compact morphology and volume swelling tendency, all of the surface area available is not accessible to electrolyte ions resulting in poor cyclic ability. Also, the dopant used in most of the cases are HCl and H_2SO_4 which are strong and highly corrosive in nature resulting in degradation of the polymer. A milder and less corrosive dopant such as p-toluene sulfonic acid would be advantageous for the synthesis of PANI.

Moreover, as noted from the literature, generally the specific capacitance of pure PANI is in low-moderate range with lower specific energy and power density values. These properties may be improved by combining pure PANI with other materials.

Out of all the literature studied, PANI nanofibers, incurred a maximum specific capacitance of 832 Fg^{-1} followed by PANI rods for 779 Fg^{-1} and PANI nanonest for 757 Fg^{-1}. The maximum specific energy was obtained at 22 Wh kg^{-1} for PANI nanofibers and at 18.8 Wh kg^{-1} in the different case of PANI nanofibers grown on graphene. The same PANI nanofibers grown on graphene also exhibited a best specific power density of 1000 W kg^{-1} and a high capacitance retention of 93 % after 10000 cycles. Further, in another research, PANI nanorods retained 96 % of its initial capacitance after 5000 cycles followed by PANI nanobridge at 88 % after 10000 cycles.

2.3 Carbon-based materials:

The materials that are most frequently used for supercapacitor electrodes are carbon-based because of their cost effectiveness, light weight, significant stability, high specific surface area, and high electrical conductivity. The carbon material can be graphene, carbon aerogel, carbide-derived carbon, carbon nanotubes, and biomass-derived activated carbon. Biomass-derived carbons are prepared by transforming natural products, including food microorganisms, animal waste, and plants, into porous carbon materials through artificial processes, thermal carbonization, and activation. The biomasses are heated at high temperatures under the protection of inert gases during the thermal carbonization process. The heteroatoms in the backbones of the biomacromolecules escape, leaving the carbon skeletons with a porous structure. The residual carbon skeletons can then be activated to form 3D interconnected structures with relatively surface area, porosity, and high conductivity, making them a great choice for supercapacitors. There are a variety of biomass resources, such as

energy crops, agricultural crops and their by-products, wood, and wood wastes, municipal and animal wastes, aquatic plants, and algae. Biomass materials are classified into four types: microorganism-based biomass, plant-based biomass, fruit and vegetable-based biomass, and animal-based biomass. Electrode materials based on biomass-derived carbon offer some crucial advantages compared to graphene and CNT, such as

(a) Cost-effectiveness: Most carbon precursors for biomass come from microbes, food and animal waste, and plant organs as they are inexpensive and plentiful.

(b) Versatility in products and processing: Using processes like carbonization, activation, and purification, different types of bioprecursors can be transformed into carbons obtained from biomass. As opposed to that, metals compounds, among other substances, can be added to the conversion procedure that enhances the carbons produced from biomass's outstanding electrochemical capacitance and catalytic abilities

(c) In-situ nanoporous structure development: while being converted to carbon under inert gas protection, the biomacromolecules' skeleton is retained, forming linked conductive properties. Environmentally friendly: Making carbons from biomass does not require harsh chemicals or high pressures, making it more energy-efficient and environmentally friendly than the procedures used to make CNT and graphene. On the other hand, utilizing biowastes as precursors to fabricate high-performance biomass-derived carbons also represents the state-of-the-art green pathway to obtain functional carbon materials.

However, biomass-derived carbon materials are generally utilized to synthesize composite materials in combination with suitable metal oxides and/ or conducting polymers to achieve desirable electrochemical results as they lack sufficient energy density. These type of carbon materials also help regulate the morphologies and size by scattering them over porous support/skeleton due to volumetric fluctuations

Manasa et al. [97] derived carbon from recycled jute and activated it with KOH which showed a specific capacitance of 346 Fg^{-1} in 6 M KOH at a current density of 1 Ag^{-1}. The cyclic stability was found to be close to 96 % over 10000 cycles. Yu et al. synthesized cheese-shaped porous carbon from *Juncus Effuses. L*. (JEL) as raw material was activated by K_2CO_3 for 24 h and then carbonized in an inert atmosphere for 2 h. The prepared carbon material incurred a specific capacitance of 357 Fg^{-1} at 1 Ag^{-1} and 280 Fg^{-1} at 20 Ag^{-1} [98]. In another research, Wei et al. developed hierarchically interconnected porous carbon through the pyrolysis of *Rhus typhina* fruits followed by KOH activation. The prepared electrode displayed a specific capacitance of 568 Fg^{-1} at 1 Ag^{-1} and 99 % of capacitance retention after 10000 cycles at 30 Ag^{-1} [99]. Khan et al. obtained inexpensive rod-like porous carbon from tea-waste and extracted a specific capacitance of 332 Fg^{-1} at 1 Ag^{-1} and 222 Fg^{-1} at 100 Ag^{-1} with a loss of 2.2 % of its initial capacitance after 100000 cycles at 100 Ag^{-1} [100]. In another study, Bao et al. synthesized a cauliflower-derived nitrogen-doped hierarchical porous carbon with the help of KOH activation. The fabricated electrode exhibited 311 Fg^{-1} at 1 Ag^{-1} and 250 Fg^{-1} at 50 Ag^{-1} in 6 M KOH electrolyte. Further, the assembled supercapacitor device displayed an energy density and power density of 20.5 $Whkg^{-1}$ and 448.8 Wkg^{-1} [101].

Natalia et al. studied the effect of MWCNTs as additives in glucose-derived carbons and found that a 2% addition of CNT with carbon demonstrated a specific capacitance of 206 Fg^{-1} and a rate capability of 97 % after 5000 cycles [102]. Zhu et al. derived carbon from algae microspheres grown under controlled cultivated conditions with natural intrinsic nitrogen dopant. The fabricated electrode possessed a specific capacitance of 353 Fg^{-1} at 1 Ag^{-1} with 92 % of capacitance retention after 10000 cycles at 20 Ag^{-1}. The assembled symmetric device exhibited an energy density of 20 $Whkg^{-1}$ and a power density of 332 Wkg^{-1} [103]. Karnan et al. derived activated carbon using aloe leaf (Aloe vera) as a precursor. The fabricated electrode showed a three-electrode and two-electrode specific capacitance of 410 and 306 Fg^{-1}. The

device with four cells connected in series possessed an energy density of 22.4 $Whkg^{-1}$, three times higher than that of a single cell, and a power density of 2037 Wkg^{-1} [104]. Enock et al. transformed biogas slurry into mesoporous carbon and studied the effect of activation time, temperature, and KOH/carbon mass ratio. Their research group found that the material activated at 700 °C, 3:1 KOH to carbon mass ratio, and activated for 120 min exhibited the highest specific capacitance of 289 Fg^{-1}. Based on activating temperature, the highest specific capacitance of 210 Fg^{-1} was obtained at 800 °C at an activation time of 60 min. Further, a capacitance retention of 96 % after 20000 cycles at a scan rate of 30 mVs^{-1} [105]. Jiang et al. derived porous carbon from cotton through carbonization and KOH-KnO_3 activation. The material exhibited a specific capacitance of 278 Fg^{-1} at 1 Ag^{-1} and a rate capability of 208 Fg^{-1} at 100 Ag^{-1}. It also showed a capacitance retention of 94.3 % over 10000 cycles at 100 Ag^{-1} [106]. Weimin et al. prepared porous carbon with the help of wheat straw by using citric acid as cross-linking agent and KOH for its activation. Their research group found the optimal specific capacitance of 294 Fg^{-1} and 97.6 % of capacitance retention after 5000 cycles when the quality of KOH was five times the carbonization product. The assembled symmetric supercapacitor revealed 14 $Whkg^{-1}$ energy-density and 440 Wkg^{-1} power-density [107]. Liu et al. prepared porous carbon from *eulaliopsis binate* by pyrolysis at 500 °C followed by KOH activation and used it as a supercapacitor electrode material. The reported a specific capacitance of 373 Fg^{-1} at a current density of 0.5 Ag^{-1} and 303 Fg^{-1} at 20 Ag^{-1}. The capacitance retention was found to be at 94.6 % of initial capacitance after 10000 cycles [108]. Lei and co-workers prepared CO_2-activated porous carbon aerogel from banana flesh and utilized it as a supercapacitor electrode material. The fabricated electrode exhibited a specific capacitance of 178.9 Fg^{-1} at a current density of 1 Ag^{-1} [109]. Table 2.2 presents a compilation of carbon-based materials for supercapacitor applications.

Table 2.2: Electrochemical properties of various carbon-based materials

Materials	C_{sp} (Fg^{-1})	Scan rate or Current density	E_{sp} (Wh kg^{-1})	P_{sp} (W kg^{-1})	Cycle life	Ref.
AC	334	2 Ag^{-1}	-	-	93 % when current increased by 20 times	[110]
rGO	19.5	1 Ag^{-1}	-	-	-	[111]
carbon aerogel	142.1	0.5 Ag^{-1}	19.74	500	93.9 % @ 5000 cycles	[112]
Graphene	279	0.2 Ag^{-1}			92 % @ 1000 cycles	[113]
Cotton-stalk AC	254	0.2 Ag^{-1}	18.14	450.37	96 % after 10000 cycles	[114]
Graphene films	55.3	5 mVs^{-1}	-	-	-	[115]
Solid-state Graphene films	245	1 Ag^{-1}	8.01	10.1	83 % @ 10000 cycles	[116]
Graphene hydrogel films	186	1 Ag^{-1}	0.12	460	91.6 % @ 10000 cycles	[117]
RGO	75	0.1 Ag^{-1}	-	-	91 % @ 2000 cycles	[118]
Hemp-derived AC	160	1 Ag^{-1}	19.8	21	-	[119]
RGO films	173.4 (3E)	1 Ag^{-1}	0.073 mWh cm^{-2}	3.3 Mw cm^{-2}	85.6% @10000 cycles	[120]
Human hair derived carbon flakes	340	1 Ag^{-1}	55	-	280 Fg^{-1} over 20000 cycles	[121]

Corn silk nanoporous carbon	160	1 Ag^{-1}	32.28	870.68	-	[122]
Orange peel derived carbon	407	0.5 Ag^{-1}	100.4 $\mu Whcm^{-2}$	6.7 $mWcm^{-2}$	100 % @ 5000 cycles	[123]
Porous carbon from waste shaddock endotheliums	550	0.2 Ag^{-1}	46.88	300	93.7 % @ 10000 cycles	[124]
Wax gourd derived carbon	333	1 Ag^{-1}	19.2	8625	93 % @ 5000 cycles	[125]
Lotus stem derived carbon	174	0.5 Ag^{-1}	-	-	72 % @ 10000 cycles	[126]
Jackfruit peel waste derived carbon	324	1 Ag^{-1}	-	-	93 % @ 5000 cycles	[127]
Lotus leaf derived carbon	298	20 Ag^{-1}	92	491	90 % @ 5000 cycles	[128]
Rose derived 3D carbon nanosheets	208	0.5 Ag^{-1}	20.32	525	92 % @ 10000 cycles	[129]
Porous carbon from jujube fruits	460	1 Ag^{-1}	23.7	629	94 % @ 10000 cycles	[130]
Soyabean derived porous carbon	685.1	1 Ag^{-1}	41.8	750	80 % @ 13000 cycles	[131]
Carbon from HS	194.5	0.5 Ag^{-1}	13.1	225	96 % @ 5000 cycles	[132]
Chitin derived porous carbon	245	0.5 Ag^{-1}	7.9	120	98 % @ 10000 cycles	[133]

Activated carbon from dragon fruit peels	427	5 mA cm^{-2}	112	3214	109 % @ 5000 cycles	[134]
Biomass derived carbon hooks	242.84	10 mVs^{-1}	20	1000	-	[135]

The carbon based materials have been extensively used for supercapacitor applications due to their high stability, high surface area, and high electrical conductivity such as graphene, carbon nanotubes, biomass derived carbons etc. The biomass derived carbon materials are especially cost effective and versatile in terms of synthesis and processing. It was observed from the literature available that, carbon based materials exhibit excellent specific power density and capacitance retention owing to their EDLC type behaviour but lack much behind in terms of specific capacitance and energy density. These carbon based materials when combined with other materials, act as porous support by scattering them over the skeleton and might help regulate their morphologies.

To summarize, it was observed that soyabean derived porous carbon exhibited the best specific capacitance of 685 Fg^{-1} and a capacitance retention of 80% after 13000 cycles. Also, porous carbon from Rhus typhina incurred a specific capacitance of 568 Fg^{-1} with a maximum capacitance retention of 99% after 10000 cycles and porous carbon from waste shaddock endotheliums at 550 Fg^{-1} specific capacitance. Soyabean derived porous carbon was also superior in terms of specific energy density at 41.8 Wh kg^{-1} and that from cauliflower derived porous carbon was obtained at 20.5 Wh kg^{-1}. Further the highest specific power density was observed at 8625 W kg^{-1} in the case of wax gourd derived carbon and at 2037 W kg^{-1} from activated carbon from aloe leaf. Also, a capacitance retention of 97.8 % after 100000 cycles was obtained from rod-like porous carbon from tea waste at 100 Ag^{-1}.

2.4 Metal Oxides:

Single metal oxides such as ZnO, CuO, MnO, CoO, NiO, MnO_2, RuO_2, TiO_2 etc., have been extensively used as supercapacitor electrode material in the past. However, binary metal oxides like $FeCo_2O_4$, $CuCo_2O_4$, $NiCo_2O_4$, $MnCo_2O_4$, $ZnCo_2O_4$, $CoFe_2O_4$, $CuFe_2O_4$ etc., have been shown to offer better pseudocapacitive properties due to the presence of two metal oxides within the single molecule as compared to simple metal oxides. Consequently, the binary metal oxides possess more redox active sites with multiple oxidation states [136].

The structure of metal ferrites (MN_2O_4, M, N=metal) is either spinel type or reverse spinel type. In the case of spinel type, M^{2+} - O^{2-} and Fe^{3+}-O^{2-} form face-centred cubic unit cells and occupy the tetrahedral and octahedral positions, respectively. In inverse spinel type, trivalent Fe^{3+} cations sit in tetrahedral sites completely, and M^{2+} and Fe^{3+} evenly occupy the octahedral sites. This interesting structure facilitates electron hopping between available valence states of metals and in oxygen sites and enhances electrical conductivity [137,138]. Further, it is also worth noticing that Co_3O_4 (CoO- Co_2O_3) owns a normal spinel structure where Co^{3+} and Co^{2+} sit in octahedral and tetrahedral positions, respectively. The site preference theory suggests that if we substitute transition metal oxide like Cu, Ni, Mn ($CuCo_2O_4$, $NiCo_2O_4$, $MnCo_2O_4$), then inverse spinels are formed where the foreign cation captures octahedral sites, and Co occupies both the octahedral and tetrahedral sites. In such types of structures, interconnected interstitial spaces are formed where tetrahedron shares its four apexes with the octahedron, which provides ion diffusion channels and supports hopping of charge carriers (electron or holes) between octahedral and tetrahedral sites [139,140].

Li et al. reported $MnCo_2O_4$ nanosheets that delivered a specific capacitance of 2000 Fg^{-1}at 0.5 A g^{-1} and 1150 Fg^{-1}at 20 Ag^{-1}. Their research group also reported a capacitance retention of 92.3% at 20 Ag^{-1} after 5000 cycles with an energy density of 73.95 Wh kg-1 and a power

density of 15000 W kg^{-1}[141]. Huang et al. synthesized $NiCo_2O_4$ nanoparticles for supercapacitor applications and found a specific capacitance of 429.6 Fg^{-1} at 1 Ag^{-1} (higher than NiO – 219.88 Fg^{-1} and Co_3O_4 – 294.99 Fg^{-1}) with capacitance retention of 74.3 % at 16 Ag^{-1} compared with 1 Ag^{-1} and 88.54 % retention after 4000 cycles [142]. Dong et al. prepared $MnCo_2O_4$ nanocage through dual metal ZIF which exhibited a specific capacitance of 1763 Fg^{-1} at 1 $Ag^{-1,}$ and after 4500 cycles, a capacitance retention of 95 % was reported at 1 Ag^{-1} of current density. Also, the fabricated electrode exhibited 54.15 Wh kg^{-1} energy-density and 5026.5 W kg^{-1} power-density [143]. Marabet et al. prepared $ZnCo_2O_4$, $NiCo_2O_4$, $MnCo_2O_4$, and $CuCo_2O_4$ spinels by sol-gel method and reported specific capacitance of 151 Fg^{-1}, 211 Fg^{-1}, 158 Fg^{-1}, and 285 Fg^{-1}, respectively. Aparna et al. reported that the binary metal oxides $NiFe_2O_4$, $MnFe_2O_4$, $ZnFe_2O_4$, and $CuFe_2O_4$ demonstrated better electrochemical properties than their individual metal oxides [138]. Jin et al. prepared copper-cobalt hybrid oxide that manifested better electrochemical performance than their single metal oxides due to synergistic effects of Cu_2O and CoO [144]. Chen et al. prepared porous $NiCo_2O_4$ flower-like nanostructures for supercapacitor electrode material and found a specific capacitance of 658 Fg^{-1} at 1 $Ag^{-1,}$ two folds higher than that of NiO and Co_3O_4. $NiCo_2O_4$ also demonstrated capacitance retention of 93.5 %s after 10000 cycles with energy-density of 28.2 Wh kg^{-1} and peak power density of 13875 W kg^{-1} [145]. Table 2.3 depicts a detailed summary of the literature based on binary metal oxides and their composites.

Table 2.3: Electrochemical properties of metal oxides for supercapacitors

Materials	C_{sp} (Fg^{-1})	Scan rate or Current density	E_{sp} (wh kg^{-1})	P_{sp} (w kg^{-1})	Cycle life	Ref.
$NiMn_2O_4$	202	0.5 $mAcm^{-2}$	28.055	1125	-	[146]
$CoFe_2O_4$	777.4	0.5 $mAcm^{-2}$	17	3277	125 % after 1500 cycles	[147]

$FeCoO_4$	428	5 mVs^{-1}	23	3780	97 % @1500 cycles	[148]
$ZnMoO_4$	234.75 (SC)	0.5 Ag^{-1}	20.808	199.44	82 % @1600 cycles	[149]
$CuCo_2O_4$	338 (3E)	1 Ag^{-1}	3.05	22110	77 % @1000 cycles	[150]
$MnCo_2O_4$	290 (3E)	1 mVs^{-1}	10.04	5200	98% @1000 cycles	[151]
$ZnCo_2O_4$	1625 (3E)	5 Ag^{-1}	12.5	6400	94% @5000 cycles	[152]
$CoFe_2O_4$	65.5 (SC)	10 mVs^{-1}	8.51	1020	90.9 % @10000 cycles	[153]
$NiFe_2O_4$	137.2	4 Ag^{-1}	16.9	-	100 % @100 cycles	[154]
$CuCo_2O_4$/ rGO	2064	2 Ag^{-1}	77.2	953	96 % @5000 cycles	[155]
G/PPy/ $MnFe_2O_4$	147.2	10 mVs^{-1}	-	-	95 % @1000 cycles	[156]
$CoFe_2O_4$	132.94	5 mVs^{-1}	6.731	47	-	[157]
$CoFe_2O_4$	461.5	1 Ag^{-1}	33.5	727.8	95.8 % @5000 cycles	[158]
$MnZnFe_2O_4$	783	5 mVs^{-1}	76.5	3700	57.5 % @2000 cycles	[159]
$MnFe_2O_4$	97.1	0.1 Ag^{-1}	-	-	76 % @2000 cycles	[160]
$NiFe_2O_4$	562.1	4 Ag^{-1}	34.91	1100	80.3 % @1500 cycles	[161]
$MnFe_2O_4$	58.2	0.1 Ag^{-1}	-	-	49.3 % @2000 cycles	[162]
$NiFe_2O_4$/ G	207	5 mVs^{-1}	-	-	95 % @1000 cycles	[163]

Metal oxides such as CuO, ZnO, MnO_2 and especially RuO_2 offer high specific capacitance due to their ability to undergo reversible redox reactions. This allows for the storage of more charge per unit area or volume compared to materials in addition to a comparatively wider potential window. However, the binary metal oxides, have been shown to offer better electrochemical properties due to the presence of more redox active sites. On the other hand, the cost of these materials are significantly high due to complex synthesis processes, and they also suffer from limited cycle life as a result of structural changes over a period of time.

It is evident from the literature review that, these materials can offer good specific capacitance and energy density but lack behind in terms of capacitance retention. These binary metal oxides when combined with other materials such as conducting polymer and carbon based materials might overcome this limitation due to the synergistic effects of all the materials.

Out of the literature studied, the $MnCo_2O_4$ nanosheets incurred a highest specific capacitance of 2000 F g^{-1}. The binary composite $CuCo_2O_4$/ rGO exhibited a specific capacitance of 2064 Fg^{-1} with an exceptional specific energy density of 77.2 Wh kg^{-1}. Also, $CoFe_2O_4$ incurred specific capacitance of 777.4 Fg^{-1} with astounding specific power density of 22100 W kg^{-1}. In terms of capacitance retention, $NiCo_2O_4$ showed a capacitance retention of 93.5 % after 10000 cycles followed by CoFe2O4 with 90.9 % after 10000 cycles.

2.5 Composite materials

The combination of a conducting polymer, carbon-based material, and metal oxide in composite materials has demonstrated enhanced electroactivity compared to pure materials. Further, it is not feasible to fabricate electrodes that exhibit all the positive effects such as high specific capacitance, high power density, high energy density, and high cyclic stability from a single material. Therefore, the strategy of developing hybrid composite materials by combining different species uses their advantageous characteristics has shown promising results.

Several references highlighting these observations have been discussed below:

Ghosh et al. fabricated MnO_2@PANI/ 3D graphene foam-based all-solid-state asymmetric supercapacitor, exhibiting a specific capacitance of 82.1 Fg-1 at 0.5 Ag-1 with an energy density of 22.3 $Whkg^{-1}$ at 5 Ag^{-1}. A capacitance retention of 89 % was observed after 5000 cycles [164]. Palsaniya et al. prepared a symmetric tandem supercapacitor using PANI-RGO-ZnO nanocomposite by varying the ratio of PANI and ZnO and keeping the RGO constant. It was found that the nanocomposite PANI-RGO-ZnO 2:1 (PANI-ZnO) possessed a higher surface area which is attributed to excellent ionic diffusion and specific capacitance. A specific capacitance of 40 Fg^{-1} at 0.05 Ag^{-1}. The fabricated symmetric supercapacitor device demonstrated a specific energy-density and power density of 5.61 $Whkg^{-1}$ and 402 Wkg^{-1}. A capacitance retention of 86 % was observed after 5000 cycles at 100 mVs^{-1} scan rate [165]. Raghavan et al. synthesized graphene/PANI/CuCr2O4-based nanocomposite as electrode material which showed a specific capacitance of 443.4 Fg^{-1} at 1 Ag^{-1}. After 10000 cycles, a capacitance retention of 92 % was reported [166]. Yoruk et al. prepared a supercapacitor electrode based on graphene oxide/ TiO_2/ polyaniline and used the device for energy storage application for electrical circuit. They used different proportions of graphene oxide, TiO_2, and aniline monomer in the ratio of 1:5:1, 1:5:2, 1:5:3, 1:5:4, 1:5:5. The highest specific capacitance of 692.87 Fg^{-1} at 2 mVs^{-1} was incurred by the material prepared with 1:5:4 proportions, respectively. The highest energy density and power density were found to be at 7.79 $Whkg^{-1}$ and 8910 Wkg^{-1}. The different ternary nanocomposites displayed capacitance retention of 100 %, 95.8 %, 86.5 %, 85.55 %, and 76 % after 1000 cycles [167]. Jeyaranjan et al. synthesized ternary hierarchical microspheres from PANI/rGO/CeO_2, exhibiting a specific capacitance of 684 Fg^{-1} at 1 Ag^{-1} in 1 M H_2SO_4. A capacitance retention of 92 % was obtained after 6000 cycles at 4 Ag^{-1}. The fabricated asymmetric device exhibited specific energy density and power density of 46.27 $Whkg^{-1}$ and 850 Wkg^{-1} [168]. Bai et al. prepared composite by following a

facile two-step approach from MoS_2/rGO/PANI, including hydrothermal and in-situ polymerization. The fabricated electrode showed a specific capacitance of 570 Fg^{-1} at 1 Ag^{-1} and 78.6 % of capacitance retention after 500 cycles at 1 Ag^{-1} [169]. Xie et al. produced rGO-CeO_2/porous PANI using a three-step process and optimized the composition of the ternary composite in terms of mass ratio. Their study revealed that the composite rGO-CeO_2/porous PANI reached a maximum capacitance of 454.8 Fg^{-1} at 1 Ag^{-1} when the CeO2 and porous PANI mass ratio 1:4. The specific capacitance retention of the material was found to be 70.23 % after 10000 cycles at 5 Ag^{-1} [170]. Ma et al. developed a ternary composite based on polyaniline/ graphene oxide/ copper. Their research concluded that when the mass fraction of GO/Cu was 10 %, the specific capacitance could reach 557.92 Fg^{-1} at 1 Ag^{-1}. With an increase in this mass fraction beyond 10 %, the specific capacitance started decreasing as the electric double layer of graphene dominated. They also reported specific capacitance of pristine polyaniline and GO as 289 and 180 Fg^{-1}, respectively [171]. Thakur et al. investigated the electrochemical performances of ternary composite based on PANI-CNT-MoS_2 and reported a specific capacitance of 350 Fg^{-1} at 1 Ag^{-1} for 5% MoS_2, which was higher than the individuals. When MoS_2 was 2.5% and 10% in the ternary composite, they observed lesser specific capacitance of 320 Fg^{-1} and 240 Fg^{-1}, respectively. 2.5% of MoS_2 was not much effective in overcoming pore blockages of PANI due to agglomeration of CNT and, therefore, could not surmount ion exchange hindrance. However, MoS_2 with 5 weight percentage optimized the available surface area, and ion exchange took place seamlessly between PANI and the electrolyte, and in turn, increased the capacitance. With the increase in MoS_2 weight percentage to 10%, the specific capacitance decreased, which could be due to the active pore blockage by the surplus amount of MoS_2 particles. More MoS_2 could be tightly packed on the surface of PANI, thereby inhibiting proper ion exchange between PANI and the electrolyte [172]. Zha et al. studied ternary $MnFe_2O_4$-carbon black-polyaniline and obtained the highest specific

capacitance of 204.3 F/g, which was better than that of carbon black (57.1 Fg^{-1}), $MnFe_2O_4$-carbon black (26.8 F/g), and carbon black-PANI (161.4 Fg^{-1}). They described that the presence of PANI offered developed conductive pathways for the movement of charges inside the electrode and restricted the volume change and aggregation of $MnFe_2O_4$. Carbon black provided a large surface area to $MnFe_2O_4$ and PANI for uniform deposition and avoided the destruction of electrode material. $MnFe_2O_4$ facilitated intimate interaction among the participating constituents of the ternary hybrid due to its ability to create a bridge between them. This ensured continuous and effective charge transport [173]. Shabani et al. synthesized a ternary nanocomposite of PANI/RGO/Au nanoparticles that exhibited outstanding capacitance of 303 Fg^{-1}, as compared to 190 Fg^{-1} for pristine PANI [174]. Naderi et al. reported that carbon black-graphite-MnO_2-based ternary system recorded higher current responses than individual systems. The enhanced current could result from a synergistic effect between carbon black, graphite, and MnO_2 [175]. Sankar et al. revealed that a ternary hybrid composite of $MnFe_2O_4$/graphene/polyaniline found that the specific capacitance of ternary material was 7.5 times that of $MnFe_2O_4$. They concluded that the outstanding electrochemical properties of ternary composite could be due to the low internal resistance, reduced diffusion length, large active sites, low diffusive resistance, and synergistic effect developed between the constituents [176]. Xiong et al. demonstrated that $MnFe_2O_4$-graphene-polyaniline (MGP) gave encouraging electrochemical properties than the binary GP, MG, MP. MGP exhibited a specific capacitance of 454.8 Fg^{-1} at 0.2 Ag^{-1} and capacitance retention of 75.8 %, which were superior to other systems. They concluded that PANI and $MnFe_2O_4$ improved the synthesized composite's electrical conductivity and enhanced the contact area between electrode and electrolyte. PANI could have provided sufficient electroactive sites for the redox transitions to occur and restricted the aggregation and dissolution of $MnFe_2O_4$. They also presumed that $MnFe_2O_4$ might be preventing the restacking of graphene [177]. Ghosh et al. studied the electrochemical

behaviors of RGO, $Ni(OH)_2$, and PANI. They reported that RGO-$Ni(OH)_2$ and $Ni(OH)_2$ had specific capacitance of 359 Fg^{-1} and 238 Fg^{-1}, respectively. The ternary system displayed an increased specific capacitance of 514 Fg^{-1} at 2 A g^{-1}. They concluded that the introduction of PANI increased the pseudocapacitive behaviour and electrical conductivity of the ternary composite [178]. Sankar et al. reported that the specific capacitance of $MnFe_2O_4$-graphene-PANI (MGP) was 338 Fg^{-1} at 0.5 mA $cm^{-2,}$ which was 10-fold of pristine $MnFe_2O_4$ electrode (32 Fg^{-1}). They suggested that the distinctively superior electrochemical properties of the ternary system were likely due to the reduction of diffusion path and internal resistance via synergistic effect. They also found that the specific capacitance and energy density were rising with the increase in graphene content for binary $MnFe_2O_4$-graphene. But, when PANI weight percentage varied from 5 to 15 % (MGP5-MGP15), the specific capacitance first increased then decreased. MGP-5, MGP-10, and MGP-15 had specific capacitances of 244 Fg^{-1}, 247 Fg^{-1}, and 240 Fg^{-1}, respectively at 5 mVs^{-1}. They suggested that at a low weight % of PANI, EDLC mechanism contributed to the capacitance (mostly). When the concentration of PANI increased, the redox reactions predominantly enhanced the capacitance [179]. Lu et al. found that Fe_3O_4/CNT/PANI composite exhibited 260 Fg^{-1} of specific capacitance, which was higher than the capacitances obtained for Fe_3O_4/CNT (208 Fg^{-1}) and Fe_3O_4 (128 Fg^{-1}). They found that PANI with 8 % (by wt) provided higher specific capacitance than PANI with 6 and 10 weight percent. The decrease in specific capacitance with an increase in PANI content could be due to the agglomeration of the particles of PANI, which would have affected the interconnection between PANI, CNT, and Fe_3O_4 and diminished the synergistic effect [180]. Wang et al. prepared supercapacitors from sulfonated graphene-MnO_2-polyaniline and obtained a capacitance of 276 Fg^{-1} at 1 Ag^{-1} which was higher than that of MnO_2/PANI (228 Fg^{-1}). They reported less IR drop (potential drop) in the case of ternary material than MnO_2/PANI, and concluded that the internal resistance decreased significantly by introducing sulfonated

graphene, and therefore, reduced the energy wastage during the charge-discharge process [181]. Xia et al. prepared a reduced graphene oxide-molybdenum oxide-polyaniline based system, which had a higher specific capacitance (553 Fg^{-1}) than MoO_3/PANI (261 Fg^{-1}) and RGO/PANI (295 Fg^{-1}) [182]. Yan et al. synthesized a ternary system of PANI-mesoporous carbon-MnO_2. The specific capacitance of PANI, PANI-mesoporous carbon, and ternary composite (12 % MnO_2) was found to be 254 Fg^{-1}, 587 Fg^{-1}, and 695 Fg^{-1}, respectively. They explained that the incorporation of MnO_2 created a larger current response in the ternary composite case, increasing the specific capacitance [183]. Lu et al. reported a ternary system of graphene-polyaniline-carbon nanotube with a specific capacitance of 569 Fg^{-1} at 0.1 A g^{-1} [184]. A detailed compilation of the ternary composite materials for supercapacitor applications has been given in Table 2.4.

Table 2.4: Electrochemical properties of various ternary composites for supercapacitors

Materials	C_{sp} (Fg^{-1})	Scan rate or Current density	E_{sp} (wh kg^{-1})	P_{sp} (w kg^{-1})	Cycle life	Ref.
PANI/g-C_3N_4@$ZnCo_2O_4$/Ni foam	24.8 (SC)	0.2 Ag^{-1}	6.35	375	100% @2000 cycles	[185]
CNF/$NiFe_2S_4$/PANI	645 (3E)	1 Ag^{-1}	22.38	125	60% @5000 cycles	[186]
MXene-CNT/PANI	429.4 (3E)	1 Ag^{-1}	-	-	93% @10000 cycles	[187]
RGO-Au@PANI	212.8 (SC)	1 Ag^{-1}	7.52	126.5	86.9% @5000 cycles	[188]
MnS/GO/PANI	207.13 (SC)	10 mVs^{-1}	18.41	-	81.6% @5000 cycles	[189]
PANI/MoS_2-MnO_2	259 (SSC)	1 Ag^{-1}	35.97	500	94.1% @4000 cycles	[190]
MnO_2/PANI/RGO	571 (3E)	1 Ag^{-1}	-	-	96.7% @10000 cycles	[191]

N-doped Graphene/$NiFe_2O_4$/PANI	667 (3E)	0.1 Ag^{-1}	23.2	27.7	90% @10000 cycles	[191]
$MnFe_2O_4$/Graphene/PANI	454.8 (3E)	0.2 Ag^{-1}	13.5	2239	76.4% @5000 cycles	[192]
MWCNTs/$FeNi_3$/PANI	398.1 (3E)	0.5 Ag^{-1}	9.1	500	80.9% @2000 cycles	[193]
Co_3O_4/PANI/Graphene	476 (3E)	2 Ag^{-1}	33.5	800	112% @3000 cycles	[194]
RGO-PANI-Fe_2O_3	605.2 (3E)	0.5 Ag^{-1}	-	-	90.6% @5000 cycles	[195]
PPY-PB-CB	163.7 (SC)	1 mVs^{-1}	18.1	10780	98.35% @2000 cycles	[196]
PANI/MnO_2/CNF	587.3	0.5 Ag^{-1}	23.3	174.9	84% @1000 cycles	[197]
PANI@Fe_3O_4@CFs	245.5 (3E)	0.5 Ag^{-1}	78.6	1047.5	82.44% @1000 cycles	[198]
PANI/Graphene/MoS_2	142.3 (SSC)	0.98 Ag^{-1}	2.65	119.21	98.11% @500 cycles	[199]
PANI-MWNTs-TiO_2	270 (SC)	0.4 Ag^{-1}	13.5	2034	67% @ 6000 cycles	[200]
PANI@MnO_2/Graphene	695 (3E)	4 Ag^{-1}	2	31200	-	[201]
PANI-TiO_2-Graphene	403.2 (3E)	2 Ag^{-1}	-	-	80% @1000 cycles	[202]
Graphene-Au-PANI	572 (3E)	0.1 Ag^{-1}	-	-	88.54% @10000 cycles	[203]

The ternary composite materials have performed better in terms of electrochemical properties as it capitalizes the advantages of individual materials. The ternary composite materials also exhibit a wide potential window which greatly boots the specific energy density of the supercapacitors. A detailed discussion on the advantages of ternary composite materials has been provided in the next section.

To summarize the findings of literature, it was observed that, PANI/MnO_2/graphene exhibited a specific capacitance of 692.87 Fg^{-1} and power density of 31200 W kg^{-1}. The ternary composite from PANI@Fe_3O_4 @ CFs incurred a highest energy density of 78.6 Wh kg^{-1} followed by PANI/rGO/CeO_2 at 46.27 Wh kg^{-1}. For capacitance retention, MnO_2/PANI/rGO at 96.7 % after 10000 cycles followed by MXene/CNT/PANI retained 93 % of initial capacitance retention and Graphene-Au-PANI at 88.54 % for the same number of cycles. It was observed that, generally the performance of ternary composite materials is better than similar constituent based binary and single materials for supercapacitor applications.

2.6 Advantages of ternary composite materials:

It is well known that conducting polymers, carbon-based materials, and metal oxides possess charge accumulation characteristics. However, due to their compact structure, metal oxides have limited anion/cation diffusion in their inner active sites as opposed to the highly wettable and polar nature of conducting polymers and carbon-based materials [204]. In general, the agglomerations of metal oxides are avoided by using conducting polymers and carbon-based materials. Less agglomeration offers larger pores, and therefore, the ionic diffusion rapidly enhances the electrochemical activities [205]. In the case of conducting polymers like polyaniline, the capacitance retention is found to be less due to hydrolysis and structural change. Due to hydrolysis, unwanted by-products are formed, which lowers the stability and conductivity. The structural change could damage the polymer backbone and decrease the active surface area. PANI and metal oxides together slow down the electrochemical kinetics, decrease the electroactive surface area, and disrupt the electrode/electrolyte interaction all at once. In order to address the issue of volumetric changes and ensure optimal performance, it is crucial to control the morphologies and sizes of composition [206]. One effective approach is

to disperse them using porous support by employing ternary composites as electrodes for supercapacitor applications. The limitations associated with the individual components can be overcome, resulting in a highly efficient system. In contrast to binary composite materials, the ternary composites generally exhibit improved specific capacitance due to the synergistic effects among the three components. The combination can result in better electron and ion transport, leading to higher capacitance values compared to binary composites. The inclusion of a third porous material can increase the surface area, providing more active sites for charge storage, thereby enhancing the overall capacitance. Ternary composites can also offer improved power density due to the optimized combination of materials that facilitate faster charge/discharge rates. Further, the energy density of ternary composites is often higher because they can combine the strengths of different materials, such as high-capacity materials and conductive materials, to store more energy. Adding a third component can also strengthen the composite's structure, resulting in enhanced long-term cycling stability and capacitance retention. This is crucial for applications such as supercapacitors and batteries, where repeated charge and discharge cycles can cause material degradation.

2.7 Research gap:

Based on the above literature survey, the research gaps are as follows:

(i) The use of low-cost waste biomass-derived carbon material, which addresses the issue of waste disposal and also eradicates the need for a conductive filler in ternary composite materials.

(ii) There is not much research on binary metal oxides of XY_2O_4 type (where X, Y are metals and O is oxygen) in ternary composites for supercapacitor applications.

(iii) Limited research has been performed on the synthesis of ternary composite material-based supercapacitor electrodes with polyaniline matrix prepared from p-toluene sulfonic acid.

(iv) While specific energy density of the best ternary composite reported (PANI@Fe_3O_4 @ CFs) is 78.6 Wh kg^{-1}, the material lags behind in terms of specific capacitance, specific power density and catacitance retention. Also, the ternary material with best specific capacitance of 695 F g^{-1}, PANI@MnO_2/Graphene, showed an energy density of only 2.0 Wh kg^{-1}. Therefore, the development of a composite material is required which fills the gap between these parameters.

(v) There is very limited research on the optimization of composite materials based on proportion of individual components.

2.8 Objectives:

(i) To explore the use of low-cost waste coconut shell-derived carbon material which acts as a porous support for other components of composite material and also acts as a separate conductive filler. Further, the carbon based materials contribute towards the EDLC type of charge storage behaviour.

(ii) To explore the use of binary metal oxides of XY_2O_4 type (where X, Y are metals and O is oxygen) in ternary composites such as $CuCo_2O_4$, $CoFe_2O_4$ and $CuFe_2O_4$. These binary metal oxides, owing to the presence of an extra metal component, contribute towards pseudocapacitive type of behaviour.

(iii) To synthesize polyaniline matrix with the help of p-toluene sulfonic acid dopant which is a milder acid as compared to HCl and leads to fewer side reactions, better thermal stability, lesser degradation during synthesis and a higher electrical conductivity polymer.

(iv) Development of cost-effective ternary composites based electrodes for supercapacitors with superior electrochemical properties of specific capacitance, specific energy-density, specific power density, cycle life, coulombic efficiency etc. above the best in the reported

literature so far. i.e. PANI/AC/ $CuCo_2O_4$, PANI/AC/ $CoFe_2O_4$ and PANI/AC/ $CuFe_2O_4$. And To study various electrochemical impedance spectroscopic characteristics such as charge transfer resistance, equivalent series resistance, and behaviour of impedance, admittance, capacitance phase angle lag vs. frequency.

(v) To optimize the ternary composite materials based on electrochemical properties using Response Surface Methodology (RSM).